Chemical Engineering Journal 355 (2019) 797–804

Contents lists available at ScienceDirect

Chemical Engineering Journal

journal homepage: www.elsevier.com/locate/cej

Selective separation of cesium contaminated clays from pristine clays by flotation

Huagui Zhang[a,*], Suparit Tangparitkul[a], Brogan Hendry[a], Joseph Harper[a], Yun Kon Kim[b], Timothy N. Hunter[a], Jae W. Lee[b], David Harbottle[a,*]

[a] School of Chemical and Process Engineering, University of Leeds, Leeds, United Kingdom
[b] Chemical and Biomolecular Engineering, Korean Advanced Institute of Science and Technology, Daejeon, Republic of Korea

HIGHLIGHTS

- Demonstration of flotation to separate cesium (Cs) contaminated clays.
- EDAB surface decoration of CS-MMT modifying particle size and wettability.
- Increased Cs contamination led to increased Cs-MMT recovery.
- Selective separation of Cs-MMT when blended with pristine-MMT.

GRAPHICAL ABSTRACT

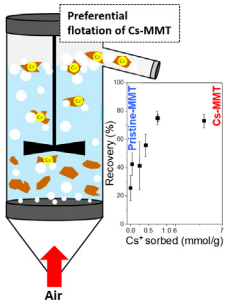

ABSTRACT

The ongoing boom of industrialization is conflicted by concerns regarding increased levels of environmental contamination, in particular the uncontrolled release of heavy metal ions and radionuclides into soils and groundwater systems. The extent of contamination can be substantial, hence ways to remediate and reduce the volume of waste for further treatment and ultimate disposal are highly desired. In the current study, flotation has been considered as an engineering solution to rapidly separate cesium contaminated clays from low-level contaminated and pristine clays. Cesium (Cs^+) sorption by montmorillonite clay particles was considered over a range of ionic concentrations (0.01–500 mM), showing a multistage sorption isotherm that can be interpreted using a two-site model, which considers both interlayer ion-exchange and specific ion sorption on the clay basal planes at higher cesium concentrations. Assessment by X-ray photoelectron spectroscopy (XPS) and zeta potential confirmed the increased surface contamination with increasing Cs^+ concentration, with the surface enrichment sufficiently altering the surface chemistry of the contaminated clays for them to favourably interact with the flotation collector, ethylhexadecyldimethyl-ammonium-bromide (EDAB). Within a critical concentration range of EDAB, the cesium contaminated clays were separated from pristine clays using flotation, with recovery efficiencies of ~75% for the contaminated clays, compared to < 25% for the pristine clays. When contaminated and pristine clays were blended, separation by flotation once again demonstrated excellent selectivity for the contaminated clays. The current study highlights the potential for flotation to rapidly treat contaminated clay rich soils and significantly reduce the volume of contaminated solids for further treatment or ultimate disposal.

1. Introduction

Rapid industrial growth and the historical impact of mining, coal and the petrochemical industries, along with fertilizer, pesticide, gasoline, paint production and their use, have inadvertently contaminated the environment [1]. The level of heavy metal ion contamination in soils and groundwater systems has been reported to be as high as a few thousand mg/kg [2], and several thousand ppm [3], respectively. Moreover, the potential for radioactive contamination from the uncontrolled release of effluent or following a nuclear accident, has led to

* Corresponding authors.
E-mail addresses: hgzhang888@hotmail.com (H. Zhang), d.harbottle@leeds.ac.uk (D. Harbottle).

https://doi.org/10.1016/j.cej.2018.07.135
Received 14 May 2018; Received in revised form 17 July 2018; Accepted 19 July 2018
Available online 20 July 2018
1385-8947/

new methods being proposed to accelerate the process of environment decontamination [4–8]. The amount of contaminated land to be remediated can be vast; for example, following the incident at Fukushima in 2011, approximately 2×10^7 m^3 of soil is now classified as contaminated, which accounts for ~20% of the total waste (non-radioactive) in Japan [9]. Among the radionuclides, ^{137}Cs, being a high yield fission product of nuclear fuel, is relatively abundant in the contaminated soils and poses a substantial risk and environmental concern due to its catastrophic hazard to the biosphere and significant half-life ($t_{1/2}$ ~ 30.1 years)[10].

At present, the strategy for decontamination includes the collection of contaminated materials (e.g. surface soils, fallen leaves and branches) from inhabited areas and storage at an Interim Storage Facility (ISF). In Fukushima, by the end of 2016, approximately 230,000 m^3 of contaminated soil had been transported to the ISF. Clearly, it would be desirable to reduce the volume of waste and more importantly reduce the amount of classified contaminated waste [11]. Several methods to treat contaminated soils have been considered including i) thermal cesium removal technology [12], ii) soil washing and separation [13], and iii) decontamination of cesium contaminated soil using superconducting magnets [14], to name just a few of the piloted methods. While these studies have shown promise to decontaminate soils, it would be desirable to first reduce the volume of waste to be decontaminated by separating waste that can be classified as non-active.

While the top-soil is retrieved (approximately 80% of the deposited radionuclides were captured in the upper 2 cm of soil [15]) and stored at an ISF, it is commonly known that cesium preferentially adsorbs on clays, especially fine clays which exhibit large surface areas and a high density of charged surface sites [16–20]. It has been shown that Cs-contaminated materials collected from around Fukushima were mostly clay of partially-vermiculitized biotite termed 'weathered biotite' (WB), and aluminous smectite which was found in abundance [21,22]. Moreover, it was reported that clays account for approximately 7% of the top-soil (depth < 10 cm), as sampled near to the Fukushima site, with most of the remaining soil components being silt and sands that are poor sorbers of radionuclides [15]. Hence, methods to recover and separate contaminated clays from the remaining materials are highly desired.

Separation and treatment of contaminated materials has significance during site remediation, for example, large decommissioning programs such as that at the Sellafield site (UK), where Cs levels in a number of site wastes are reported to be in the concentration range of 0.01 and 20 mM [18,23]. A wide range of contamination concentrations have been considered (up to 1000 mM Cs^+ solution for 1 y to predict long-term effects) [18,24], with different strategies ensuring contamination of the clay frayed edge, Type II and clay surface planar sites. For illite, contamination of the planar sites has been reported for Cs concentrations as low as 10^{-6} mol/L [15].

Froth flotation, an engineering solution frequently adopted by the mining industry to separate target minerals from waste gangue [25], is being considered to separate contaminated clays from uncontaminated materials to facilitate significant waste volume reduction. Flotation has previously been used to separate fines contaminated by plutonium, uranium or heavy metals from clean, larger soil-particles, resulting in good separation efficiencies [26,27]. Furthermore, flotation has been used to treat trace elements directly from aqueous wastes with the aid of an ionic surfactant to concentrate and extract non-active ions of opposite charge at the liquid/gas interface [28]. The process has been combined with a pre-precipitation step to enable flotation of the poorly soluble Cs complexes. For example, sodium tetraphenylborate (NaTPB) is added to form cesium tetraphenyl-borate(CsTPB) which is floated to decontaminate the aqueous phase [29].

Based on those previous demonstrations, flotation is being considered in the current study to selectively separate Cs-loaded (contaminated) clays (Cs-MMT) from uncontaminated clays (MMT). Natural grade montmorillonite (MMT) was used throughout the study and was chosen due to its high cation exchange capacity (CEC) and high ion adsorption site density, both contributing to substantial Cs sorption [30,31]. Flotation has been considered for MMTs of varying Cs contamination levels. Cs sorption by MMT was studied across a range Cs^+ concentrations (0.01–500 mM), with two-site modelling and a range of analytical techniques used to verify the sorption mechanism(s). Flotation in the presence of a collector (ethylhexadecyldimethyl-ammonium-bromide [EDAB]) has been demonstrated with the mechanism for selective separation understood from the physicochemical characterization of MMT and Cs-MMTs.

2. Experimental

2.1. Materials

Naturally occurring MMT of ~200 mesh (< 74 μm) was purchased from Alfa Aesar and used without washing. Cesium chloride (CsCl) and methyl isobutyl carbinol (MIBC) of analytical grade were purchased from Sigma-Aldrich. Ethylhexadecyldimethyl-ammonium-bromide (EDAB, M_w 378.5 g/mol, purity > 98.0%) was purchased from Merck Millipore. Ultrapure Milli-Q water with a resistivity of 18.2 MΩ·cm was used throughout the study.

The cation exchange capacity (CEC) of MMT was measured to be 90 meq./100 g solids, using 0.01 M Cu(II)-triethylenetetramine complex $[Cu\ Trien]^{2+}$ as the index adsorption cation, and the complex concentration measured at 577 nm by UV spectroscopy (UV-1800, Shimadzu, Japan)[8]. The BET specific surface area of MMT was 29.85 m^2/g, determined by N_2 adsorption analyzer (TriStar 3000, Micromeritics, US). The chemical composition of MMT was determined by X-ray fluorescence (XRF) spectrometry (Primus II, Rigaku, Japan) and found to be 2.20 wt% Na_2O, 2.39 wt% MgO, 20.80 wt% Al_2O_3, 66.86 wt % SiO_2, 0.06 wt% P_2O_5, 0.40 wt% SO_3, 0.70 wt% K_2O, 1.66 wt% CaO, 0.16 wt% TiO_2, 0.05 wt% MnO, 4.57 wt% Fe_2O_3, 0.03 wt% CuO, 0.01 wt% ZnO, 0.06 wt% SrO and 0.05 wt% ZrO_2.

2.2. Batch sorption of Cs^+

All batch sorption studies were completed using plastic containers (polypropylene) to prevent Si contamination from glassware and potential Cs^+ adsorption onto glass, as highlighted in an earlier study [32]. 0.4 g MMT was dispersed in 20 mL CsCl solution (20 g/L in Milli-Q water at neutral pH) with the Cs^+ concentration ranging from 0.01 to 500 mM, diluted from a 1000 mM CsCl stock solution. 100 mL CsCl stock solution was prepared beforehand by dissolving 16.836 g CsCl solid in Milli-Q water (neutral pH) at room temperature. The suspensions were then placed on an orbital shaker at 150 rpm for 48 h at room temperature before centrifuging at 7000*g* (relative centrifugal force) for 15 min. The supernatant was decanted and passed through a 0.45 μm syringe filter before measuring the Cs^+ concentration by Atomic Adsorption Spectrophotometry (AAS, Varian 240FS spectrometer, Agilent, US) at wavelengths of 852.1 nm and 455.5 nm, based on a calibration curve established from dilutions of the 1000 mg/L CsCl standard solution. The sorbed Cs^+ concentration by MMT, q (mmol/g), was determined using the following equation:

$$q = \frac{(C_0 - C_e)V}{m} \quad (1)$$

where C_0 and C_e (both in mmol/L) are the initial and equilibrium Cs^+ concentrations, respectively (determined by AAS), V (L) the volume of the suspension, and m (g) the amount of adsorbent (MMT). All sorption tests were repeated in triplicate with supernatants analysed three times using AAS. Average values are reported along with error bars to show the experimental variability.

2.3. Sorption modelling

Cs^+ sorption modelling was performed with the aid of the PHREEQC2 code [33]. The ion exchange reaction between cation B with charge z_B that exists in the aqueous solution, and cation A with charge z_A at the cation exchange sites of the clay (MMT) is expressed as follows [16]:

$$z_B\text{Clay(A)} + z_A\ B \leftrightarrow z_A\text{Clay(B)} + z_B\text{A} \quad (2)$$

The cation exchange reaction can be described with selectivity coefficients, ${}_A{}^B K_{sel}$, expressed as follows [34]:

$${}_A{}^B K_{sel} = \frac{(N_B)^{z_A}(a_A)^{z_B}}{(N_A)^{z_B}(a_B)^{z_A}} \quad (3)$$

where a_A and a_B describe the activities of the cations A and B, and N_A and N_B are the equivalent fractional occupancies, defined as the sorbed quantities of the cations per mass of adsorbent (expressed in eq g^{-1}) divided by the site cation exchange capacity CEC (expressed in eq g^{-1}). The specific PHREEQC2 modelling input was edited based on the code used by Fuller et al. [18]. Briefly, the two input parameters were selectivity coefficient, K_{sel}, and sorption site capacity. The model was executed using the wateq4f.dat thermodynamic database to generate the aqueous activity coefficients [35] and calculate the site specific Cs^+ sorbed (Fig. 1). Since the fluid was Milli-Q water with Cs^+ at neutral pH, and the MMT was assumed to contain only Na^+ for simplification purposes, only three cations, H^+, Na^+ and Cs^+ were considered in the modelling.

2.4. MMT characterization

Prior to all characterization studies, the Cs-loaded MMT was extensively washed with Milli-Q water to remove excess Cs^+ following a repeated procedure of vigorous agitation to disperse the MMT followed by centrifugation (7000*g* for 15 min) to replace the supernatant. After each cycle, the Cs^+ concentration in the supernatant was measured by AAS. For ten wash cycles, the typical Cs^+ concentrations in the supernatant for MMT-Cs5mM and MMT-Cs500mM are shown in Fig. S1.

Particle/aggregate structures were visualized by depositing MMT onto an SEM stub, dried in a desiccator for 24 h and imaged using a Field Emission Gun Scanning Electron Microscope (FEG-SEM; LEO1530 GEMINI, Carl Zeiss Inc., Japan). Elemental mapping of the MMT was completed using energy dispersive X-ray spectroscopy (EDX) with an Oxford Instruments 80 mm^2 X-Max SD detector and INCA 350 software. X-ray photoelectron spectroscopy (XPS, Sigma probe, Thermo Fisher Scientific, US) was performed with a monochromated Al Kα X-ray source. Powder X-ray diffraction (XRD) patterns were obtained using a X-ray diffractometer (D8, Bruker, US) fitted with a LynxEye detector, using a Cu Kα (1.54 Å) radiation source operating at 40 kV and 40 mA, calibrated against a silica standard. Each sample was scanned over a 2θ range of 4° to 49.98° with a step size of 0.03299° at 2 s per step.

2.5. Zeta potential

The MMT zeta potential was measured using the acoustic zeta probe analyser (Colloidal Dynamics, USA). MMT suspensions were prepared to 0.16 w/w% at near neutral pH (pH 7–8) and stirred at 300 rpm for the duration of the test. The zeta potential of Cs-loaded MMT was measured following the titration of 10 mM EDAB. The suspension was stirred for 5 min following each EDAB titration to ensure an equilibrium condition had been reached.

2.6. Contact angle

The droplet three-phase contact angle on pristine and Cs-loaded MMT compressed pellets was approximated by the sessile drop technique (Attension Theta, Biolin Scientific, Sweden). Using a 2-ton load, MMT particles were compressed into a circular pellet with a surface area of 13 mm^2. A ~10 µL droplet of 0.18 mM EDAB solution was deposited on the MMT pellet with the time-dependent droplet contact angle and droplet penetration into the pellet (Fig. S2) determined by image analysis using the Attension Software.

2.7. Particle size

A FlowCam VS benchtop system (FlowCam® VS, Fluid Imaging Technologies, USA), equipped with a 100 µm flow cell (FC-100) and a 10× magnification lens (Olympus®, Japan) was used to measure the particle size distributions of pristine and Cs-loaded MMT. Prior to measurement, the FlowCam system was repeatedly flushed with Milli-Q water ensuring no debris/contamination in the flow cell. Pristine MMT and MMT-Cs50mM particles (1 g/L) were conditioned separately with a specified concentration of EDAB for 5 min before priming the flow cell. For analysis, a flow rate of 0.1 mL/min was chosen for suspensions with low EDAB concentrations (c.a. $<$ 0.5 mM), while 3.0 mL/min was used for high EDAB concentrations (c.a. $\geq$ 0.5 mM) due to the presence of larger aggregates. Images of the particles/aggregates in the flow cell were captured by a high-resolution digital camera at 10 fps. A minimum of 10,000 particles/aggregates were counted for each measurement and a minimum of five measurements were performed, with representative data plotted as a histogram.

2.8. QCM-D

Quartz Crystal Microbalance with Dissipation monitoring (QCM-D E4, Q-Sense, Biolin Scientific, Sweden) was used to measure EDAB adsorption onto pristine and Cs-loaded MMT. Using the spin coating technique, a thin layer of MMT was formed on the Al_2O_3 sensor (f_0 = 5 MHz) by depositing 10 droplets of 10 ppm MMT or Cs-MMT suspension (pH = 4.0) onto the QCM sensor rotating at 1200 rpm for 2 min. The particle layer was then dried at room temperature overnight before being used for QCM-D measurement. Prior to each particle deposition, new QCM sensors were sonicated in 50 mM CTAB, rinsed with excess ethanol, dried using compressed air, exposed to UV ozone for 10 min and rinsed with Milli-Q water before drying with compressed air. All measurements began by pumping Milli-Q water (0.4 mL/min) through the flow cell to establish stable baselines (frequency and dissipation) before 0.18 mM EDAB solution was continuously pumped for 1 h. Changes in the frequency (ΔF) and dissipation (ΔD) were continuously measured across several frequency overtones with only the third overtone used for data analysis due to its good signal-to-noise ratio. All measurements were conducted at 22 °C.

2.9. Flotation

The washed Cs-loaded MMT was stored as a 20 g/L stock suspension to avoid sample drying and the clumping of MMT. Flotation tests were performed by pouring 30 mL stock suspension (equivalent to 0.6 g solids) into a laboratory-scale flotation cell (column diameter and height: 65 mm and 97 mm), with flotation bubbles generated at the column base through a sintered glass plate with micron-sized pores. A schematic of the flotation set-up is provided in our previous study [8]. Milli-Q water was then added to the MMT suspension to increase the total volume to 210 mL. Agitation of the MMT suspension was provided by a ¾ inch, 4-blade, 45° pitched impeller rotating at 300 rpm, and the air flowrate was fixed at 2 mL/min. A specified volume of 10 mM EDAB was added to the MMT suspension and mixed for 5 min. For flotation, the stirrer speed was reduced to 100 rpm and a given volume of MIBC frother added to the suspension. Increasing the air flowrate to 7 mL/min, MMT froth was recovered through a side-arm in the flotation cell and collected in a 200 mL beaker. Flotation tests proceeded for 10 min with the remaining froth and residual particles in the side-arm collected. The foams were dried at 90 °C and weighed (m_d in g). Particle

recovery (R %) was calculated using $R\% = m_d/m_0 \times 100\%$, where m_0 is the initial particle mass in the suspension. Each experiment was repeated a minimum of three times.

3. Results and discussion

3.1. Cs^+ sorption by MMT

Fig. 1 shows the Cs^+ sorption isotherm for MMT with the sorbed amount q (mmol/g) given as a function of the equilibrium solution concentration C_e (mM). For discussion, the sorbed isotherm is also shown as a function of the initial solution concentration C_0 (mM) as shown inset. Multistage Cs^+ sorption was observed with q gradually increasing with increasing C_0 (low C_0 c.a. ≤ 10 mM), reaching a pseudo-plateau at intermediate C_0 (c.a. 10–100 mM), before increasing once again at high C_0 (c.a. ≥ 100 mM). As previously reported [18,36], those changes in the sorption isotherm indicate the existence of two or more sorption sites with distinctive exchange energies. For MMT, the multi-site sorption includes the high affinity sites such as the Frayed Edge (FE) and 'Type II' sites related to the interlayer and the high capacity planar site [16,18,37]. A two-site model was proposed to describe the observed multistage sorption behaviour. Site I describes the ion-exchange within the MMT interlayer, high affinity with a site adsorption capacity assumed to be comparable to the CEC of MMT (i.e. 90 meq/100 g, ~0.90 mmol Cs^+/g), and Site II describes the surface adsorption relating to Cs^+ interaction with surface silanol or alumino groups (i.e. –SOH + Cs^+ = SOCs + H^+), with a site adsorption capacity, for modelling purposes, simplified to be the maximum sorption capacity measured within the studied concentration range, that is, ~7.52 mmol Cs^+/g, and a selectivity coefficient comparable to the surface complexation[38], log K_{sel} ~ −1.0. The model parameters are provided in Table 1.

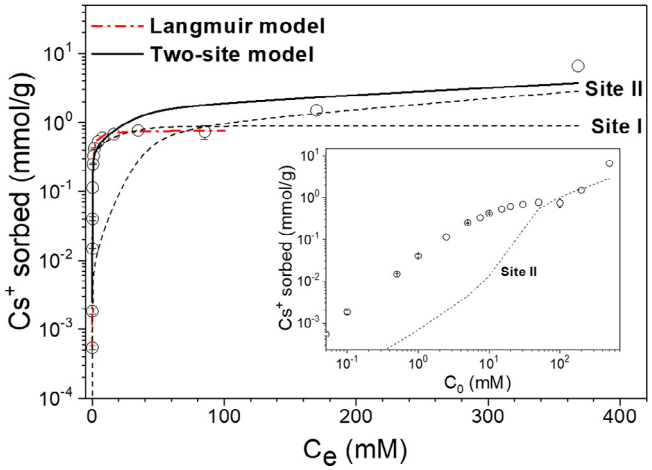

Fig. 1. Cs^+ sorption by MMT (q) as a function of the equilibrium Cs concentration (C_e) (open symbol: experimental data). The solid line represents the theoretical Cs^+ sorbed using the two-site model which is a function of the site specific sorption, Site I – interlayer and Site II – surface (dash lines). The red dot-dash line is the Langmuir model fit. Inset: Cs^+ sorption by MMT as a function of the initial Cs concentration (C_0).

Table 1
Parameters used for the two-site model.

	Site capacity (mmol Cs^+/g)	Selectivity coefficient log K_{sel}[a]	
		H^+	Cs^+
Site I	0.90	1.8[b]	1.8 [39]
Site II	7.52	2.5 [18]	−1 [38]

[a] log K_{sel} is a relative value of the exchange ion normalized against Na^+.
[b] equivalent to Cs^+ as described in reference [18].

Fig. 1 shows reasonable agreement between the experimental data and the simplistic two-site (Sites I and II) model, with Cs^+ sorption at low C_0 (or C_e) dominated by Site I (interlayer), and sorption at Site II (surface) becoming more prevalent with increasing C_0 (or C_e), especially when C_0 exceeds 10 mM (i.e. C_e > ~1.60 mM). Further improvement to the model is needed to provide greater accuracy when predicting the complex sorption behaviour at high C_0.

For low C_0 when Cs^+ sorption predominantly occurs via MMT interlayer, Cs^+ sorption can be well described by the Langmuir model, which assumes a monolayer sorption, finite number of binding sites and uniform sorption energies (Fig. 1), and is given by

$$q = \frac{bq_m C_e}{1 + bC_e} \quad (4)$$

where the fitting parameter b is the Langmuir constant and relates to the affinity of the binding sites (L $mmol^{-1}$), and q_m the maximum sorption capacity that describes the efficiency of Cs^+ removal from solution at or near saturation. The equilibrium concentration, C_e (mmol L^{-1}), is the Cs^+ concentration remaining in solution following sorption. The Langmuir model gives $q_m = 0.775$ mmol/g and $b = 0.6911$ L $mmol^{-1}$ with a coefficient of determination (R^2) of 0.91.

The washed Cs-contaminated MMTs (i.e. Cs-MMT) were characterized by XPS. In the survey spectra (Fig. 2a), peaks of Cs $3d_{5/2}$ at

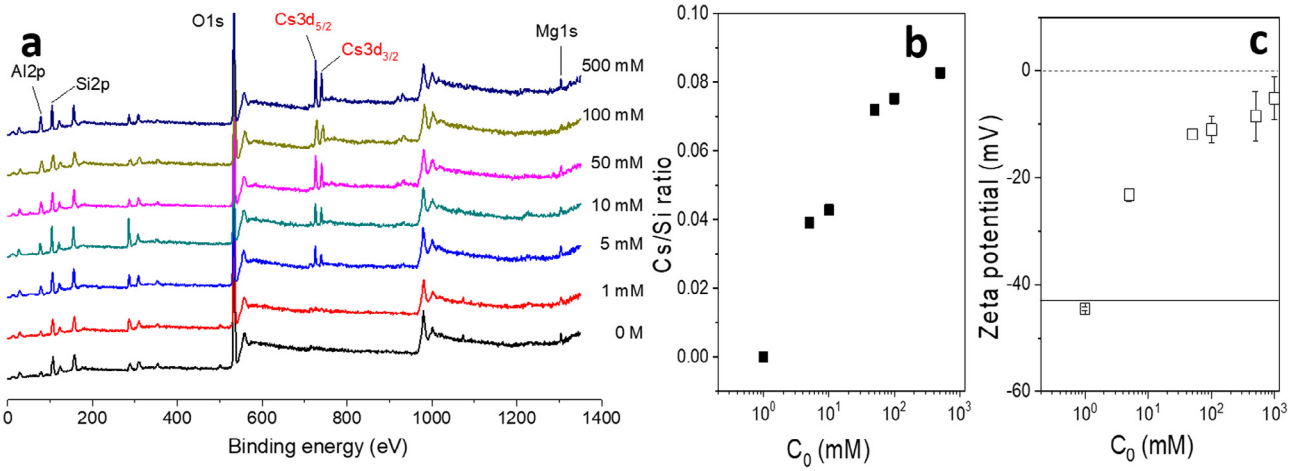

Fig. 2. a) XPS spectra of pristine MMT and Cs-MMTs (C_0 labelled for each spectra); b) corresponding Cs/Si ratio quantified from the XPS peak area; c) zeta potential of Cs-MMTs. Solid line: zeta potential of pristine MMT.

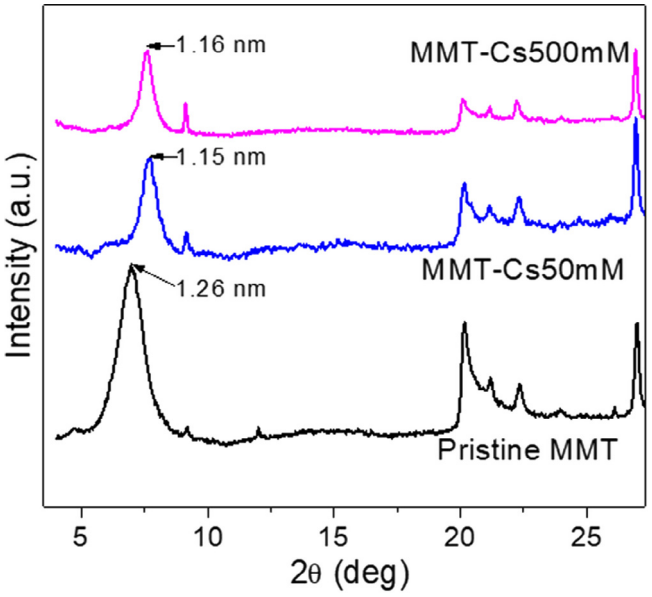

Fig. 3. XRD spectra of pristine MMT and Cs-MMTs.

~725.5 eV and Cs $3d_{3/2}$ at ~740.0 eV were identified for Cs-MMT when prepared in solutions of $C_0 \geq 5$ mM, contrasting the absence of such peaks at lower C_0. Additionally, from the Cs/Si ratio (which was quantified based on the peak areas of Cs $3d_{5/2}$ and Si 2p (Fig. 2b)) the increased intensity of the Cs characteristic peaks corresponded to increasing C_0, with such behavior in excellent agreement with the two-site model (Fig. 1), confirming significant surface adsorption when $C_0 > 10$ mM. It is worth noting that the adsorbed Cs was very stable to washing in Milli-Q water with negligible Cs^+ released from Cs-MMT following 10 consecutive washes (Fig. S1).

For smectite minerals such as MMT, isomorphic substitutions occur in both the tetrahedral (Al^{3+} for Si^{4+}) and octahedral (Mg^{2+} for Al^{3+}) sheets. Substitution in the octahedral sheet results in a delocalized permanent charge [40], while the presence of compensating ions on the tetrahedral sheet weaken the interlayer binding, such that the compensating ions become available for ion exchange, thus MMT exhibits a high ion exchange capacity. The 2:1 structure leads to surface charge anisotropy with a negative silica basal plane, and a pH dependent alumina edge (positive for pH < 8) [40].

As shown in Fig. 2c, the apparent zeta potential (ζ) of pristine MMT was −43 mV. Following Cs^+ sorption ($C_0 \geq 5$ mM) and Cs-MMT washing, the zeta potential of Cs-MMT progressively decreased, almost neutralizing when $C_0 > 100$ mM. Such behavior validates the Site II sorption mechanism at higher C_0. Any influence of the electrolyte concentration is considered to be negligible since all Cs-MMTs were extensively washed in Milli-Q water.

The Cs-MMT powder XRD patterns are shown in Fig. 3. For pristine MMT, the peak observed at 7.0° corresponds to the (0 0 1) basal plane with an interlayer spacing of 1.26 nm. The interlayer spacing of Cs-MMT was greatly reduced when MMT was contaminated by high Cs levels (C_0 50 mM and C_0 500 mM), with the (0 0 1) basal plane peak shifted to $2\theta \sim 7.6°$, corresponding to a basal plane spacing of ~1.16 nm. Following saturation with Cs^+, the MMT interlayer collapsed, due to Cs^+ shedding its hydration shell upon entering the MMT interlayer [41,42]. Such mechanism was also confirmed by the increasing intensity of the 2θ peak observed at 9.1° which corresponds to a d-spacing of 0.97 nm, characteristic of a fully collapsed interlayer of smectite [43].

3.2. Interaction between MMT/Cs-MMT and EDAB

Cationic surfactants adsorb onto MMT via electrostatic interaction, decorating the particle to modify surface charge and wettability [44]. In the current study, EDAB, an alkylammonium cationic surfactant (C16 hydrocarbon chain), was selected following an optimization study. When adding a surfactant to Cs-MMT, some Cs^+ is likely desorbed, i.e. surfactant washing. At the surfactant concentration used in the flotation study (see below), the total Cs^+ removed was < 15% and thus considered insignificant, see Fig. S3.

To determine collector-particle interaction the zeta potential of Cs-MMTs was measured as a function of the EDAB concentration (0 mM to 1.0 mM, relative to 1 g/L MMT), as shown in Fig. 4a. As expected, addition of EDAB led to charge neutralization of Cs-MMTs and in most cases charge reversal at higher EDAB concentrations, the one exception being pristine MMT. As previously shown (XPS, zeta potential, EDX), surface contamination of MMT by Cs was measurable when $C_0 \geq 5$ mM, with the extent of contamination a function of C_0. The critical EDAB concentration for charge neutralization decreased with increasing Cs contamination. For all Cs-MMTs, the zeta potentials were bounded by two plateau regions at low and high EDAB concentrations. The low concentration plateau would be indicative of EDAB adsorption via the MMT interlayer [31,45], and then surface adsorption following interlayer site saturation, an effect which is enhanced in the presence of increased Cs contamination. EDAB progressively saturates the surface

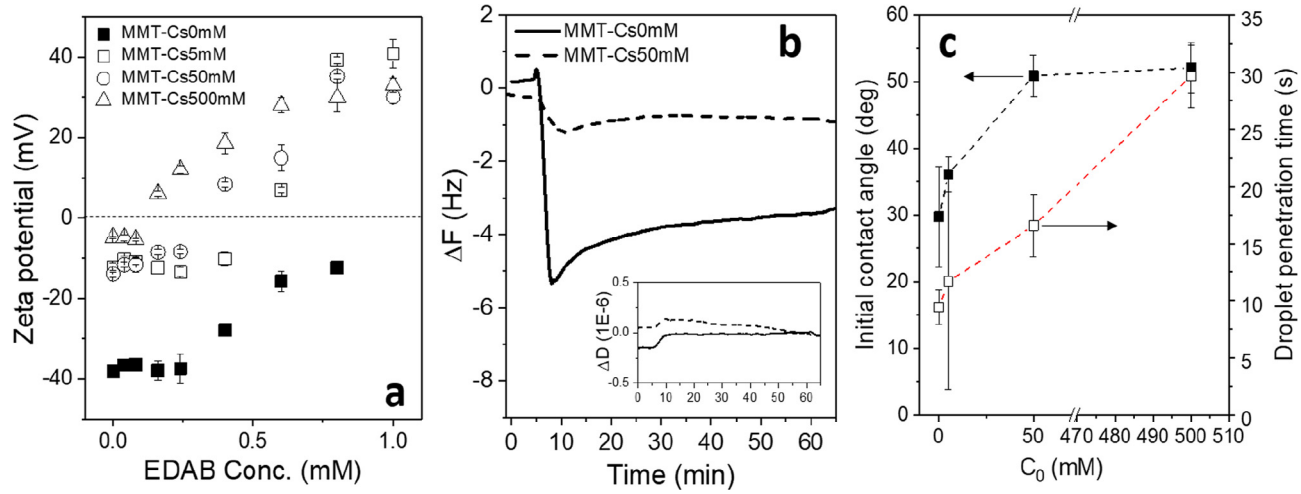

Fig. 4. a) Zeta potentials of pristine MMT and Cs-MMTs as a function of the added EDAB concentration; b) QCM-D data confirming adsorption of EDAB (0.18 mM) onto surfaces of pristine MMT and MMT-Cs50mM; c) initial droplet (0.18 mM EDAB) contact angle and liquid penetration time as a function of Cs contamination level (Cs-MMT pellet).

sites leading to charge neutralization/ reversal with a second plateau due to the formation of a bilayer.

Interaction between EDAB and MMT/Cs-MMT was also verified by QCM-D. As shown in Fig. 4b, EDAB deposits on both pristine MMT and Cs-MMT (C_0 = 50 mM) with negligible changes in sensor dissipation, hence the deposited layer is very thin. The EDAB deposited mass can be approximated by the Sauerbrey [46] equation ($\Delta m = -c\Delta f/n$), where c is the mass sensitivity constant (18 $ng.cm^{-2}.Hz^{-1}$ at 5 MHz), n the overtone number (n = 3), and Δf the change in sensor resonance frequency (Hz). Based on the frequency shifts (MMT, $\Delta f = -5.3$ Hz; Cs-MMT, $\Delta f = -1.2$ Hz) the Sauerbrey mass equalled 31.8 ng/cm^2 and 7.2 ng/cm^2 for the pristine MMT and Cs-MMT, respectively. A lower EDAB deposited mass on Cs-MMT was measured indicating a charge screening by Cs^+, inhibiting adsorption of the cationic molecule. However, even when the MMT surface was highly contaminated the flotation collector still interacted with Cs-MMT.

For flotation the target particles must be sufficiently hydrophobic to interact with the rising air bubbles. While it is challenging to measure the wettability of an individual particle, various methods have been proposed for pseudo-quantitative assessment of particle wettability [47]. Fig. 4c shows the initial contact angle and the droplet penetration time measured using the compressed disc method. Due to issues associated with MMT swelling, the data should only be used as a qualitative measure of wettability changes. A general trend of droplet contact angle and droplet penetration time increasing with Cs contamination of MMT was observed. Increasing droplet contact angle would suggest surface decoration of Cs-MMT by EDAB, in good agreement with the zeta potential data. As such the Cs-MMT should be more favourable to float than MMT.

Particle/aggregate sizes of pristine MMT and Cs-MMT (Fig. 5) in the presence of EDAB (0 to 0.5 mM) were measured using the FlowCam VS. In the absence of EDAB, the average particle sizes were 2.47 ± 0.47 μm and 2.56 ± 0.16 μm for pristine MMT and Cs-MMT (C_0 = 50 mM), respectively, and showed very similar polydispersity indexes (PDIs). Such similarity confirmed that the MMT particles were not affected by Cs contamination and washing protocol, also supported by the SEM images in Fig. S4. Fig. 5 provides an assessment of the number of particles per mL of liquid and the equivalent spherical diameter (ESD). When considering MMT, it is readily evident that EDAB has minimal effect on the particle/aggregate sizes until an EDAB concentration of 0.5 mM. At the highest EDAB concentration, the size distribution was broadened and the number of particle counts decreased which confirmed the formation of larger aggregates. For Cs-MMT, the addition of 0.05 mM EDAB began to aggregate the fines as shown by the slight broadening at ESD > 3 μm. Further increases in the EDAB concentration led to larger aggregates with typical structures shown in the FlowCam images, see Fig. S5.

3.3. Flotation of MMT and Cs-MMT

The flotation of MMT and Cs-MMT (C_0 = 50 mM) was compared for an equivalent collector dosage (0.18 mM EDAB relative to 1 g/L solids) and increasing frother (MIBC) volume, see Fig. 6a. Both samples showed improved recovery with increasing frother volume, yet the Cs-MMT recovery always exceeded that of MMT. Superior flotation of Cs-MMT was underlined by complete recovery of Cs-MMT at a frother vol./solids ratio of 250 μL/g. The result validates flotation as a method to separate highly contaminated clays from pristine clays. However, it is unlikely that such separation would be so discrete and a gradient of contaminated particles would more likely be encountered. For Cs-MMT of varying contaminations, the flotation method was repeated at a fixed frother amount (116.67 μL/g solids) and EDAB concentration (0.18 mM), and the recovery of Cs-loaded MMTs compared in Fig. 6b. While the recovery of pristine MMT was ~25%, particle recovery was observed to increase as the particle contamination level increased. Particle recovery plateaued at ~75% when the degree of Cs contamination was greater than ~0.74 mmol/g (i.e. $C_0 \geq$ 50 mM), with the three Cs-MMTs (highest levels of contamination) demonstrating similar levels of surface contamination as shown in Figs. 2b and c. Following 10 min flotation, the suspensions were visually compared (Fig. 6c), with the suspension turbidity observed to decrease with increasing levels of Cs contamination, validating the flotation performance. The particle dispersion at low Cs levels (0 and 1 mM) appeared finer with larger aggregates formed when Cs-MMT ≥5 mM, in good agreement with the particle size data (Fig. 5). These findings suggest that the mechanism for enhanced recovery results from the combined effects of increased hydrophobicity and aggregate size (i.e. akin to floc-float [44,48])

When blending MMT and Cs-MMT (C_0 = 50 mM) the flotation recovery showed good agreement with the linear additive rule (Fig. 7), where the relative recovery of the pristine MMT and Cs-MMT were taken as the linear extremes, thus confirming the preferential flotation of Cs-MMT. Preferential recovery was further validated by EDX mapping the floated particles for the Cs element (inset Fig. 7). The increased color intensity and Cs/Si ratio confirmed the recovered particles to be Cs-MMT.

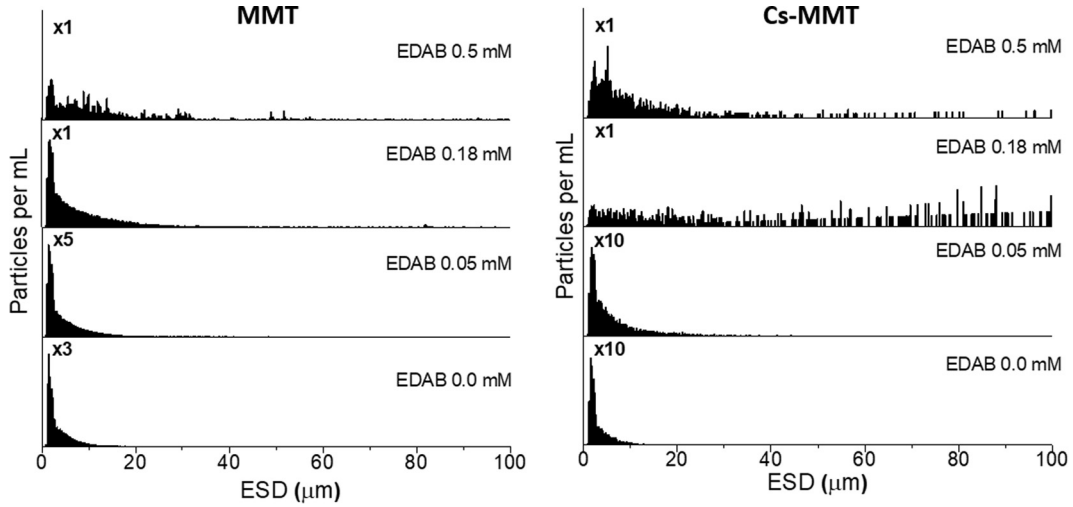

Fig. 5. Histogram of particles per mL and equivalent spherical diameter (ESD) for pristine MMT and Cs-MMT (C_0 = 50 mM) as a function of the EDAB concentration, from bottom to top: 0 mM, 0.05 mM, 0.18 mM and 0.5 mM. Multiplication factors indicate the relative change in particles per mL.

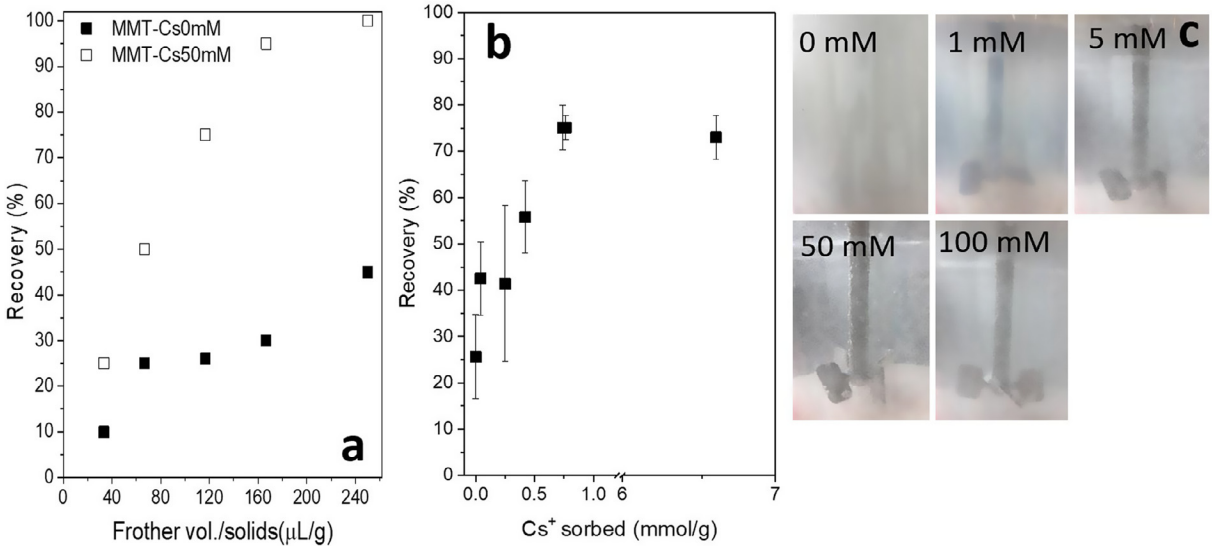

Fig. 6. Flotation recovery of pristine MMT and Cs-MMT in the presence of 0.18 mM EDAB and as a function of a) added frother (μL/g solids), b) Cs contamination of MMT (frother/solids ratio, 116.67 μL/g) (corresponding C_0 of Cs from left to right: 0, 1, 5, 10, 50, 100 and 500 mM), and c) images of the particle suspension following 10 min flotation, C_0 labelled inset (images correspond to Fig. 6b).

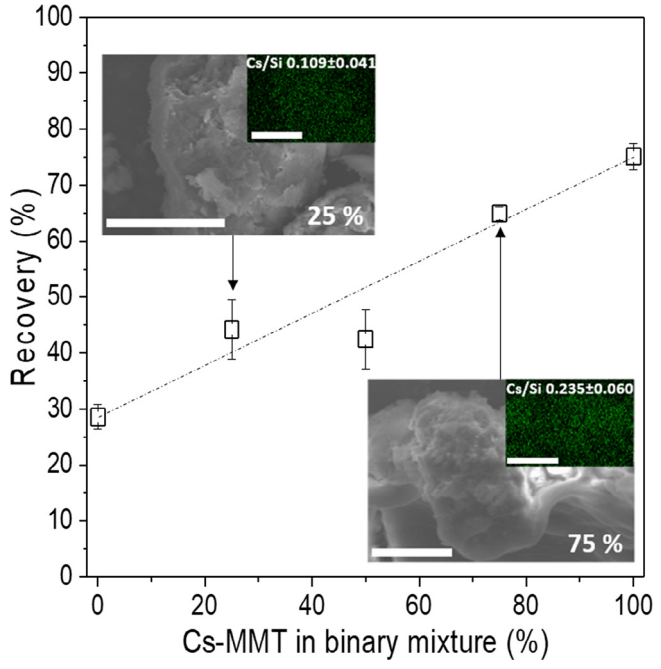

Fig. 7. Flotation recovery from a blend of pristine MMT and Cs-MMTs (C_0 = 50 mM, 0.18 mM EDAB, frother = 116.67 μL/g solids). Dash line represents the linear additive rule based on the flotation performance of pristine MMT and Cs-MMT. Inset: SEM images of the floated particles with EDX mapping of the Cs element shown inset. All scale bars = 10 μm.

4. Conclusion

Uncontrolled release of heavy metal ions and radionuclides and their gradual accumulation in soils and groundwater systems can lead to an environmental hazard. Much effort has been dedicated to the treatment and clean-up of water systems with wide-ranging extraction methods adopted. Treatment of soils has been less considered, and the problem to successfully remediate is often thought to be more challenging. One complexity relates to the "targeting" and separation of contaminated solids, with the aim to significantly reduce the volume of waste needed to undergo further treatment and preparation for ultimate disposal.

Cs^+ sorption by MMT can be described using both Langmuir and two-site models, with the Langmuir model more applicable at lower C_0 when interlayer Cs^+ sorption predominates, and the two-site model better describing Cs^+ sorption on the planar sites of MMT. XPS analysis confirmed detectable levels of Cs surface contamination at C_0 = 5 mM, with the Cs/Si ratio asymptotically limiting when $C_0 \geq 50$ mM. MMT contamination was shown to be stable with Cs levels remaining after 10 consecutive washes. While the particle size and size distribution were unaffected by the Cs levels, the apparent surface charge of MMT decreased with increasing Cs. EDAB was chosen as an appropriate flotation collector for Cs-MMT. Cs-MMTs required a lower concentration of EDAB to neutralize the apparent surface charge. The EDAB concentration dependence was exploited to preferentially float Cs-MMT. Dosing the particle suspensions with 0.18 mM EDAB and 116.67 μL MIBC/g solids, flotation recoveries of pristine and Cs-MMT (C_0 = 50 mM) were ~25% and ~75%, respectively, showing a clear preference to recover Cs-MMT. Even at low Cs contamination levels (C_0 = 1 mM) the particle recovery exceeded that of pristine MMT. Flotation of blended (MMT and Cs-MMT) samples confirmed the preferential flotation of Cs-MMT with flotation recoveries in good agreement with the linear additive rule.

Methods to recover contaminated solids using high-throughput engineering solutions are highly desired. By favorable modification of aggregate size and particle wettability, the current study has provided proof-of-concept demonstration to preferentially separate Cs-MMTs from pristine MMT. With easy deployment and high throughputs, flotation columns may prove advantageous to accelerate some of the large scale remediation programs and minimize the volume of waste sent for ultimate disposal.

Data statement

Huagui Zhang, Suparit Tangparitkul, Brogan Hendry, Joseph Harper, Yun Kon Kim, Timothy N. Hunter Jae W. Lee, David Harbottle (2018): Data associated with 'Selective separation of cesium contaminated clays from pristine clays by flotation' University of Leeds. [Dataset]. https://doi.org/10.5518/430, Article metadata is available under a Creative Commons Attribution licence (CC-BY).

Acknowledgements

This work was financially supported by the Engineering and Physical Sciences Research Council (EPSRC) (EP/M026426/1) and the National Research Foundation of Korea (NRF) (NRF-2015M2A7A1000219).

Appendix A. Supplementary data

Supplementary data associated with this article can be found, in the online version, at https://doi.org/10.1016/j.cej.2018.07.135.

References

[1] M.P.S.R. Matos, A.A.S. Correia, M.G. Rasteiro, Application of carbon nanotubes to immobilize heavy metals in contaminated soils, J. Nanopart. Res. 19 (2017) 126.
[2] I. Maiz, I. Arambarri, R. Garcia, E. Millan, Evaluation of heavy metal availability in polluted soils by two sequential extraction procedures using factor analysis, Environ. Pollut. 110 (2000) 3–9.
[3] F.L. Fu, Q. Wang, Removal of heavy metal ions from wastewaters: A review, J. Environ. Manage. 92 (2011) 407–418.
[4] D.H. Ding, Z.Y. Zhang, Z.F. Lei, Y.N. Yang, T.M. Cai, Remediation of radiocesium-contaminated liquid waste, soil, and ash: a mini review since the Fukushima Daiichi Nuclear Power Plant accident, Environ. Sci. Pollut. R 23 (2016) 2249–2263.
[5] S. Baik, H. Zhang, Y.K. Kim, D. Harbottle, J.W. Lee, Enhanced adsorption capacity and selectivity towards strontium ions in aqueous systems by sulfonation of CO2 derived porous carbon, RSC Adv. 7 (2017) 54546–54553.
[6] Y. Kim, Y.K. Kim, S. Kim, D. Harbottle, J.W. Lee, Nanostructured potassium copper hexacyanoferrate-cellulose hydrogel for selective and rapid cesium adsorption, Chem. Eng. J. 313 (2017) 1042–1050.
[7] Y.K. Kim, T. Kim, Y. Kim, D. Harbottle, J.W. Lee, Highly effective Cs+ removal by turbidity-free potassium copper hexacyanoferrate-immobilized magnetic hydrogels, J. Hazard. Mater. 340 (2017) 130–139.
[8] H.G. Zhang, Y.K. Kim, T.N. Hunter, A.P. Brown, J.W. Lee, D. Harbottle, Organically modified clay with potassium copper hexacyanoferrate for enhanced Cs+ adsorption capacity and selective recovery by flotation, J. Mater. Chem. A 5 (2017) 15130–15143.
[9] Ministry of the Environment, Progress on Off-site Cleanup Efforts in Japan Available: http://josen.env.go.jp/en/documents/ (April 2015).
[10] S.B. Yang, C. Han, X.K. Wang, M. Nagatsu, Characteristics of cesium ion sorption from aqueous solution on bentonite- and carbon nanotube-based composites, J. Hazard. Mater. 274 (2014) 46–52.
[11] Ministry of the Environment, Progress on Off-site Cleanup and Interim Storage Facility in Japan Available: http://josen.env.go.jp/en/ (April 2017).
[12] D. Parajuli, H. Tanaka, Y. Hakuta, K. Minami, S. Fukuda, K. Umeoka, R. Kamimura, Y. Hayashi, M. Ouchi, T. Kawamoto, Dealing with the Aftermath of Fukushima Daiichi nuclear accident: decontamination of radioactive cesium enriched ash, Environ. Sci. Technol. 47 (2013) 3800–3806.
[13] M. Hirose, Y. Kikawada, A. Tsukamoto, T. Oi, T. Honda, K. Hirose, H. Takahashi, Chemical forms of radioactive Cs in soils originated from Fukushima Dai-ichi nuclear power plant accident studied by extraction experiments, J. Radioanal. Nucl. Ch 303 (2015) 1357–1359.
[14] Y. Yoshida, K. Sekiya, N. Nomura, F. Mishima, Y. Akiyama, S. Nishijima, Study on volume reduction of contaminated soil by radioactive cesium using magnetic separation, IEEE T Appl. Supercon. 25 (2015) 3700505.
[15] H. Kato, Y. Onda, M. Teramage, Depth distribution of Cs-137, Cs-134, and I-131 in soil profile after Fukushima Dai-ichi Nuclear Power Plant Accident, J. Environ. Radioactiv. 111 (2012) 59–64.
[16] A. Benedicto, T. Missana, A.M. Fernandez, Interlayer collapse affects on cesium adsorption onto illite, Environ. Sci. Technol. 48 (2014) 4909–4915.
[17] L. Dzene, E. Ferrage, J.C. Viennet, E. Tertre, F. Hubert, Crystal structure control of aluminized clay minerals on the mobility of caesium in contaminated soil environments, Sci. Rep-Uk 7 (2017) 43187.
[18] A.J. Fuller, S. Shaw, C.L. Peacock, D. Trivedi, J.S. Small, L.G. Abrahamsen, I.T. Burke, Ionic strength and pH dependent multi-site sorption of Cs onto a micaceous aquifer sediment, Appl. Geochem. 40 (2014) 32–42.
[19] A.J. Fuller, S. Shaw, M.B. Ward, S.J. Haigh, J.F.W. Mosselmans, C.L. Peacock, S. Stackhouse, A.J. Dent, D. Trivedi, I.T. Burke, Caesium incorporation and retention in illite interlayers, Appl. Clay Sci. 108 (2015) 128–134.
[20] A.W. Miller, Y.F. Wang, Radionuclide interaction with clays in dilute and heavily compacted systems: a critical review, Environ. Sci. Technol. 46 (2012) 1981–1994.
[21] H. Mukai, S. Motai, T. Yaita, T. Kogure, Identification of the actual cesium-adsorbing materials in the contaminated Fukushima soil, Appl. Clay Sci. 121 (2016) 188–193.
[22] E. Fujii, K. Tamura, T. Hatta, H. Yamada, T. Yaita, T. Kogure, Cesium sorption to paddy soil in Fukushima, Clay Sci. 19 (2015) 17–22.
[23] NDA, Sellafield High, Level Liquid Waste Inventory 2D02, (2007).
[24] T. Missana, A. Benedicto, M. Garcia-Gutierrez, U. Alonso, Modeling cesium retention onto Na- K- and Ca-smectite: Effects of ionic strength, exchange and competing cations on the determination of selectivity coefficients, Geochim. Cosmochim. Ac 128 (2014) 266–277.
[25] T.T. Chau, W.J. Bruckard, P.T.L. Koh, A.V. Nguyen, A review of factors that affect contact angle and implications for flotation practice, Adv. Colloid Interfac. 150 (2009) 106–115.
[26] U.S. Department of Energy, Heavy Metals Contaminated Soil Project, Resource Recovery Project, and Dynamic Underground Stripping Project: Technology Summary, DOE/EM-0129P (February 1994).
[27] U.S. Environmental Protection Agency, Technology Screening Guide for Radioactively Contaminated Sites, EPA 402-R-96-017 (November 1996).
[28] C. Micheau, A. Schneider, L. Girard, P. Bauduin, Evaluation of ion separation coefficients by foam flotation using a carboxylate surfactant, Colloid Surface A 470 (2015) 52–59.
[29] M.A. Soliman, G.M. Rashad, M.R. Mahmoud, Fast and efficient cesium removal from simulated radioactive liquid waste by an isotope dilution-precipitate flotation process, Chem. Eng. J. 275 (2015) 342–350.
[30] H. Long, P.X. Wu, N.W. Zhu, Evaluation of Cs+ removal from aqueous solution by adsorption on ethylamine-modified montmorillonite, Chem. Eng. J. 225 (2013) 237–244.
[31] T.H. Wang, C.J. Hsieh, S.M. Lin, D.C. Wu, M.H. Li, S.P. Teng, Effect of alkyl properties and head groups of cationic surfactants on retention of cesium by organoclays, Environ. Sci. Technol. 44 (2010) 5142–5147.
[32] J. Chorover, S.K. Choi, M.K. Amistadi, K.G. Karthikeyan, G. Crosson, K.T. Mueller, Linking cesium and strontium uptake to kaolinite weathering in simulated tank waste leachate, Environ. Sci. Technol. 37 (2003) 2200–2208.
[33] D.L.A. Parkhurst C.A.J., User's guide to PHREEQC(Version 2), US Geological Survey 1999 Denver.
[34] G.L. Gaines, H.C. Thomas, Adsorption studies on clay minerals. 2. A formulation of the thermodynamics of exchange adsorption, J. Chem. Phys. 21 (1953) 714–718.
[35] J.W. Ball, Nordstrom. D.K.,, User's manual for WATEQ4F with revised thermodynamic database and test cases for calculating speciation of major, trace and redox elements in natural waters., Open-File Report 91-183. USGS,Denver (1991).
[36] Q.H. Fan, M. Tanaka, K. Tanaka, A. Sakaguchi, Y. Takahashi, An EXAFS study on the effects of natural organic matter and the expandability of clay minerals on cesium adsorption and mobility, Geochim. Cosmochim. Ac 135 (2014) 49–65.
[37] M.H. Bradbury, B. Baeyens, A generalised sorption model for the concentration dependent uptake of caesium by argillaceous rocks, J. Contam Hydrol. 42 (2000) 141–163.
[38] B. Grambow, M. Fattahi, G. Montavon, C. Moisan, E. Giffaut, Sorption of Cs, Ni, Pb, Eu(III), Am(III), Cm, Ac(III), Tc(IV), Th, Zr, and U(IV) on MX 80 bentonite: an experimental approach to assess model uncertainty, Radiochim. Acta 94 (2006) 627–636.
[39] B.C. Bostick, M.A. Vairavamurthy, K.G. Karthikeyan, J. Chorover, Cesium adsorption on clay minerals: An EXAFS spectroscopic investigation, Environ. Sci. Technol. 36 (2002) 2670–2676.
[40] E. Tombacz, M. Szekeres, Colloidal behavior of aqueous montmorillonite suspensions: the specific role of pH in the presence of indifferent electrolytes, Appl. Clay Sci. 27 (2004) 75–94.
[41] R.M. Cornell, Adsorption of cesium on minerals – A review, J Radioan. Nucl. Ch. Ar 171 (1993) 483–500.
[42] J.J. Wu, B. Li, J.L. Liao, Y. Feng, D. Zhang, J. Zhao, W. Wen, Y.Y. Yang, N. Liu, Behavior and analysis of Cesium adsorption on montmorillonite mineral, J. Environ. Radioactiv. 100 (2009) 914–920.
[43] Z. Yermiyahu, I. Lapides, S. Yariv, Thermo-XRD-analysis of montmorillonite treated with protonated Congo-red. Curve fitting, Appl. Clay Sci. 30 (2005) 33–41.
[44] J.C.M. Chapelain, S. Faure, D. Beneventi, Clay flotation: effect of TTAB cationic surfactant on foaming and stability of illite clay microaggregates foams, Ind. Eng. Chem. Res. 55 (2016) 2191–2201.
[45] M.J. Sanchez-Martin, M.C. Dorado, C. del Hoyo, M.S. Rodriguez-Cruz, Influence of clay mineral structure and surfactant nature on the adsorption capacity of surfactants by clays, J. Hazard. Mater. 150 (2008) 115–123.
[46] G. Sauerbrey, Verwendung Von Schwingquarzen Zur Wagung Dunner Schichten Und Zur Mikrowagung, Z. Phys. 155 (1959) 206–222.
[47] T. Dang-Vu, R. Jha, S.Y. Wu, D.D. Tannant, J. Masliyah, Z.H. Xu, Wettability determination of solids isolated from oil sands, Colloid Surf. A 337 (2009) 80–90.
[48] D.G. Devivo, B.L. Karger, Studies in flotation of colloidal particulates – Effects of aggregation in flotation process, Separ Sci 5 (1970) 145–167.